View metadata, citation and similar papers at core.ac.uk
brought to you by CORE
provided by DSpace@MIT

PHYSICAL REVIEW B **93**, 035455 (2016)

Negative compressibility in graphene-terminated black phosphorus heterostructures

Yingying Wu,[1] Xiaolong Chen,[1,2] Zefei Wu,[1] Shuigang Xu,[1] Tianyi Han,[1] Jiangxiazi Lin,[1] Brian Skinner,[3] Yuan Cai,[1] Yuheng He,[1] Chun Cheng,[4] and Ning Wang[1,*]

[1]*Department of Physics and the William Mong Institute of Nano Science and Technology, Hong Kong University of Science and Technology, Hong Kong, China*
[2]*Department of Engineering and Cambridge Graphene Centre, University of Cambridge, 9 J. J. Thomson Avenue, Cambridge CB3 0FA, United Kingdom*
[3]*Massachusetts Institute of Technology, Cambridge, Massachusetts 02139, USA*
[4]*Department of Materials Science and Engineering and Shenzhen Key Laboratory of Nanoimprint Technology, South University of Science and Technology, Shenzhen 518055, China*

(Received 13 September 2015; published 29 January 2016)

Negative compressibility is a many-body effect wherein strong correlations give rise to an enhanced gate capacitance in two-dimensional (2D) electronic systems. We observe capacitance enhancement in a newly emerged 2D layered material, atomically thin black phosphorus (BP). The encapsulation of BP by hexagonal boron nitride sheets with few-layer graphene as a terminal ensures ultraclean heterostructure interfaces, allowing us to observe negative compressibility at low hole carrier concentrations. We explain the negative compressibility based on the Coulomb correlation among in-plane charges and their image charges in a gate electrode in the framework of Debye screening.

DOI: 10.1103/PhysRevB.93.035455

I. INTRODUCTION

Negative compressibility in an electronic system describes the effect of electron-electron (*e-e*) interaction, which lowers the potential of electrons when the carrier density of a system increases [1–4]. This effect provides a new strategy to enhance the gate capacitance of field-effect transistors (FETs) beyond the expected geometric capacitance for low-power dissipation [1,5–8]. The effects of negative compressibility have been previously observed in ultraclean systems, such as in high-quality $LaAlO_3/SrTiO_3$ interfaces [9], two-dimensional (2D) GaAs systems [4,10–12], and ferroelectric materials [13], where Coulomb interactions are normally strong and play an important role in transport properties. Newly emerged 2D layered semiconductors, such as transition-metal dichalcogenides [14–18] and black phosphorus (BP) [19–28], are new platforms for both nanotechnology and fundamental physics. Among these 2D materials, atomically thin BP is a promising channel material of FETs with high mobility [24–27] and high stability by encapsulating BP with hexagonal boron nitride (BN) sheets. Our previous work has found that high-quality BN-BP-BN heterostructures with clean interfaces are ideal 2D electron systems with high mobility [25]. High-quality BN-BP-BN heterostructures also offer great opportunities to investigate quantum Hall effects [26], as well as Coulomb interactions of charge carriers in 2D materials.

In this work, we report the observation of negative electronic compressibility in BN-BP-BN capacitors constructed using few-layer graphene as terminal electrodes. Gate capacitance enhancement is apparent near the depletion region. The observation of this enhancement effect largely relies on ultraclean interfaces in BN-BP-BN heterostructures and very low impurity concentrations.

*Corresponding author: phwang@ust.hk

II. BP CAPACITOR MODEL

A simple parallel-plate capacitor structure is adopted to investigate the properties of BP. When both electrodes in a standard parallel plate capacitor are made of normal metals, the total capacitance per unit area C_t purely originates from the geometric capacitance $C_g = \frac{\varepsilon}{d}$ because the metal electrodes can perfectly screen the electric field, where ε and d are the dielectric constant and thickness of the capacitor, respectively. However, if one of the electrodes is replaced with a 2D material with finite Debye screening radius R_D, the electric field penetrates a distance R_D into the electrode [29], thereby decreasing total capacitance $C_t = \frac{\varepsilon}{d+R_D}$. On the other hand, the negative Debye screening radius is known to occur in situations where electron-electron interactions are sufficiently strong, and this gives rise to an enhanced capacitance. Such interaction-driven enhancement is often difficult to observe because of disorder effects [9,10,30].

III. EXPERIMENTS

The polymer-free dry-transfer method [31] is adopted to assemble exfoliated few-layer BP, BN, and graphene flakes into a BN-BP-BN heterostructure with few-layer graphene as a terminal electrode, as shown in Figs. 1(a) and 1(c). Annealing treatments were then conducted on the BN-BP-BN heterostructure at high temperatures up to 500 °C before metal electrode deposition was performed. BN encapsulation and annealing treatment guarantee a clean BN-BP interface with low impurity concentrations [25]. Finally, Cr/Au (2 nm/60 nm) films were deposited to form a top gate and an Ohmic contact with graphene. Polarized Raman spectroscopy was performed to characterize the properties of the few-layer BP samples. The angle-dependent Raman spectra obtained from the BP samples are shown in Fig. 1(d), which agree with previous studies [32–34].

 ©2016 American Physical Society

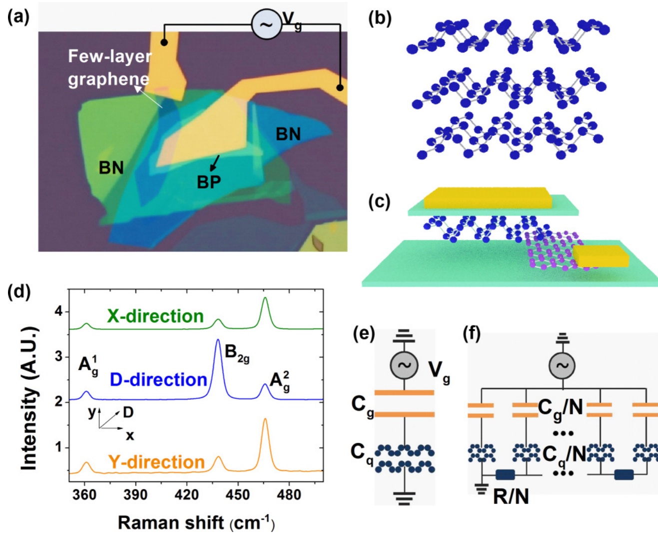

FIG. 1. BP vertical capacitor heterostructure. (a) False-color optical and (c) schematic images of the BN-BP-BN heterostructure with few-layer graphene as a terminal electrode. The BP flake is 8 nm thick, as determined using an atomic force microscope. (b) A schematic image of few-layer BP. (d) Determining the crystal orientation via Raman spectroscopy. The intensity values were normalized to the Si peak from the substrate. Equivalent circuits of the measurement setup (e) without accounting for and (f) taking into account the resistance of BP.

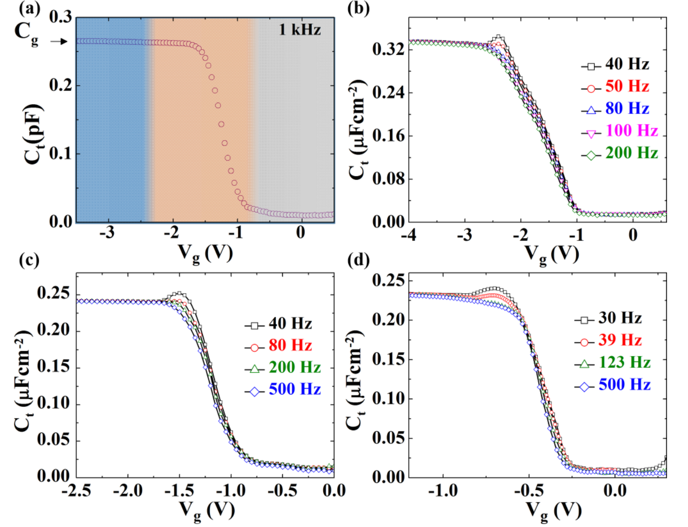

FIG. 2. Valence band of few-layer BP accessed by capacitance measurement. (a) Measured total capacitance of the 8-nm-thick sample in Fig. 1(a) (device B) with an excitation frequency of 1 kHz at 2 K. C_t as a function of the gate voltage of (b) device A with 5-nm BP and 8-nm top BN at 3 K, (c) device B with 8-nm BP and 11-nm top BN at 2 K, and (d) device C with 13-nm BP and 11.7-nm top BN at 2 K.

Using a graphene terminal to contact the BN-BP-BN heterostructure has several benefits compared with other structures (see Fig. 3 in the Supplemental Material [35]). This graphene terminal not only simplifies the fabrication procedures without a tedious chemical-etching process [36] to make contact with the encapsulated BP flakes but also ensures a polymer-free BN-BP clean interface.

The capacitance is measured between the top gate and the graphene terminal with an ac excitation frequency ranging from 20 Hz to 1 MHz [see Fig. 1(a)]. By applying a top gate voltage V_g, the Fermi energy of BP can be tuned continuously. The measured capacitance C_t is the total capacitance contributed by the two capacitors in a serial connection, as shown in Fig. 1(e). One of the capacitors is the constant geometric capacitance of the parallel-plate capacitor $C_g = \frac{\varepsilon_{\rm BN}}{d}$, where $\varepsilon_{\rm BN}$ is the dielectric constant of top BN. The other one originates from the quantum capacitance of BP, $C_q = e^2 \frac{dn}{d\mu}$ [37,38], where n and μ are the carrier density and chemical potential, respectively. Here, $\frac{dn}{d\mu}$ is the electronic compressibility, which describes the ability of an electronic system to screen external charges [4,10,12,30,39]. For ideal metals, the compressibility approaches infinity, which results in a complete screening of external charges. By contrast, $\frac{dn}{d\mu}$ is finite in low-dimensional materials, partially penetrated by the external electric field. Hence, total capacitance C_t can be expressed as

$$\frac{1}{C_t} = \frac{1}{C_g} + \frac{d\mu/dn}{e^2}. \quad (1)$$

The measured capacitance of the BN-BP-BN heterostructure with an excitation frequency of 1 kHz is shown in Fig. 2(a). Inside the band gap of BP (gray region), the total capacitance approaches zero because of the vanishing density of the states. However, when V_g is sufficiently large (blue region), the total capacitance approaches the geometric capacitance $C_t \approx C_g$, given that a larger density of states would lead to a quantum capacitance C_q much larger than C_g [9]. The total capacitance can be expressed as $C_t = \frac{\varepsilon}{d^*} = \frac{\varepsilon}{d+R_D}$ by introducing an effective thickness of the system d^*.

IV. RESULTS AND ANALYSIS

A. Enhancement of capacitance

Total capacitance C_t is evidently enhanced near the depletion region of BP at low excitation frequencies ($f < 100$ Hz). As shown in Fig. 2(b), by decreasing the excitation frequencies from 200 to 40 Hz, C_t of the 5-nm-thick BP (device A) gradually exceeds geometric capacitance C_g and shows no sign of enhancement saturation within the measured frequency range. This capacitance enhancement at low excitation frequencies is also reproducible in other devices with different BP thicknesses, as shown in Fig. 2(c) (device B with 8-nm-thick BP) and Fig. 2(d) (device C with 13-nm-thick BP). Since the mobile carrier density is strongly suppressed near the depletion, R, the resistance of BP, can reach orders of 10^3 MΩ [36]. Therefore, the capacitor is not fully charged when the excitation frequency is $f > \frac{1}{RC_t}$; thus, C_t is underestimated. The real capacitance can only be approached by lowering the excitation frequency. An equivalent circuit [Fig. 1(f)] can then be simplified into the two-serial-capacitor model shown in Fig. 1(e) when $f \ll \frac{1}{RC_t}$.

B. Negative compressibility

The enhancement of C_t ($C_t > C_g$) reveals that C_q is negative, directly proving the negative compressibility. The correlation between inverse compressibility $\frac{d\mu}{dn}$ and carrier

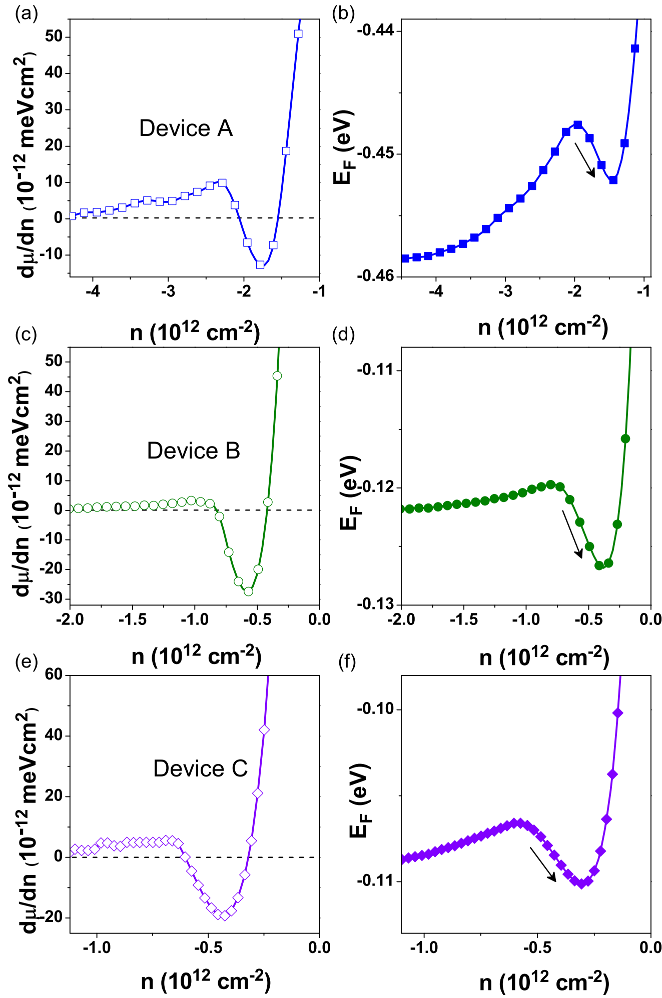

FIG. 3. Inverse of compressibility and the Fermi energy. Inverse of compressibility of devices (a) A, (c) B, and (e) C. The carrier density is determined by integrating the $C_t \sim V_g$ curve at the lowest excitation frequency, as shown in Fig. 2. The negative sign in the carrier density denotes the hole carrier density. The $E_F \sim n$ relation at (b) 3 K with an excitation frequency of 40 Hz for device A, (d) 2 K with an excitation frequency of 40 Hz for device B, and (f) 2 K with an excitation frequency of 30 Hz for device C.

density $n = \frac{C_g}{e}(V_g - V_s - V_{th})$ can be obtained through Eq. (1), as shown in Figs. 3(a), 3(c), and 3(e), where V_s and V_{th} are the surface potential of BP and the threshold voltage, respectively. V_s is extracted based on the charge conservation relation $V_s = \int_0^{V_g}(1 - \frac{C_t}{C_g})dV_g$. For device A, negative compressibility occurs at a hole carrier density of 2×10^{12} cm^{-2}, whereas negative compressibility occurs in devices B and C at a lower carrier density of below 1×10^{12} cm^{-2}. The magnitude of the effect depends on the quantity $n^{1/2}d$, so thinner BN allows us to see the negative compressibility at a higher carrier density. The Fermi energy $E_F = eV_s$ plotted as a function of gate voltage V_g of three devices is shown in Figs. 3(b), 3(d), and 3(f). The Fermi energy generally increases with the gate voltage when $C_t < C_g$. Instead, an upturn is evident in the $E_F \sim V_g$ curve, which is a signature of negative compressibility [1,12].

The negative compressibility in our system indicates the Debye screening length $R_D < 0$, which enhances the total capacitance $C_t = \frac{\varepsilon}{d+R_D}$. In the limit of the low-carrier density regime, where the average distance between two neighboring in-plane holes $n^{-1/2}$ is larger than the effective Bohr radius $a_0 = 4\pi\varepsilon\hbar^2/me^2$ of the holes in the interface, 2D holes can form a strongly correlated system dominated by the Coulomb interaction [10]. Using BP dielectric constant $\varepsilon = 12\varepsilon_0$ [40] and the effective mass of hole carriers in different layers of BP [26], a Bohr radius and the corresponding carrier density n_c can be obtained in Fig. 4(b). Hence, the BP system here (with a carrier density that is much smaller than n_c) can be regarded as a strongly correlated system. In addition, the Coulomb interactions between the holes and the image charges of the holes in the gate electrode can also significantly enhance negative compressibility, especially when $n^{-1/2} \gg d$, where $n^{-1/2}$ is the average distance between two neighboring in-plane holes [see Fig. 4(a)] [30].

C. Quantitative analysis

Analytical expressions for the effective thickness d^* have previously been derived for the case where the effective Bohr radius a_0 is much smaller than the capacitor thickness d. In this limit, the enhancement of capacitance due to correlations can be described at all densities $n \ll 1/a_0^2$ using a classical Wigner-crystal-type description. These descriptions give $d^* \approx d - 0.12n^{-1/2}$ at $n^{1/2}d \gg 1$ and $d^* \approx 2.7n^{1/2}d^2$ at $n^{1/2}d \ll 1$ [30,41]. Figure 4(c) shows the experimental data of BP compared with the theoretical function $d^*(d,n)$. The trend of the experimental data agrees well with the theoretical prediction. Deviation occurs because quantum kinetic energy is not considered in the theoretical expressions.

On the other hand, when a_0 is comparable to d, the quantum kinetic energy of the charge carriers becomes important. These quantum fluctuations weaken the strength of positional correlations and somewhat reduce the magnitude of the capacitance enhancement. This model exploits the well-studied properties of the unscreened 2D electron gas using a variational approach. To describe this effect quantitatively, we present the results for effective capacitor thickness d^*, which is related to the total energy per electron $E(n)$ by [42]

$$d^* = \frac{\varepsilon}{4\pi e^2}\frac{d\mu}{dn} = \frac{\varepsilon}{4\pi e^2}\frac{d^2}{dn^2}[E(n)n]. \tag{2}$$

Applying Hartree-Fock approximation, a simple expression with the zero-spin polarization for this correction can be derived at $n \gg 1/a_0^2$, and we get

$$d^* = d + \frac{a}{4} - \frac{1}{(2\pi)^{3/2}n^{1/2}} + \frac{d}{64\sqrt{2\pi^5}(nd^2)^{3/2}}. \tag{3}$$

The last three terms corresponds to the kinetic energy of the Fermi sea, the exchange energy of electrons, and the correction to the exchange. Results from such a model for our system are presented as the solid lines in Fig. 4(d). The theory matches the data. Notably, small deviations occur because disorder effects are not considered in the theoretical expressions, which screen Coulomb interactions among the holes. Negative compressibility could be suppressed when disorders prevail over electronic interactions. Thus, only the

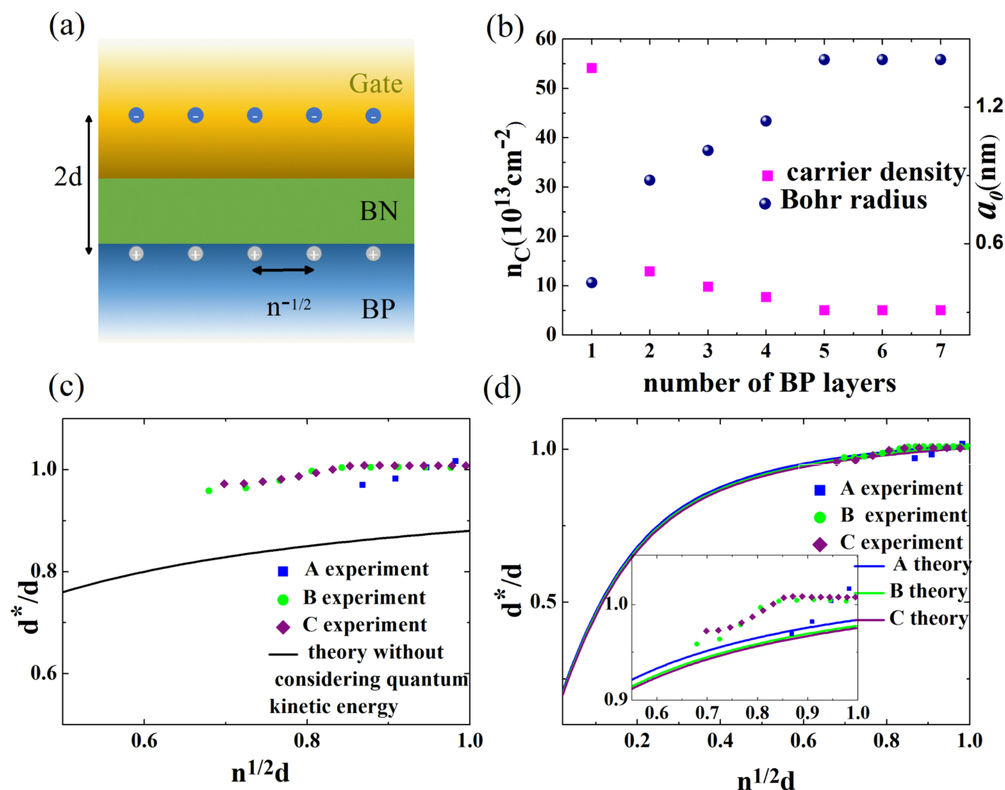

FIG. 4. Physical origin of negative compressibility detected in BP. (a) Schematic coupling of the holes in BP to the image charges of the holes in the metal electrode. Neighboring holes (white circles) in the BP formed at the BP-BN interface. The distance between two neighboring holes is $n^{-1/2}$. Negative image charges (blue circles) are formed in the metal at a distance $2d$ away from the holes, where d is the BN thickness. (b) Calculated Bohr radius of the holes in the interface and the corresponding carrier density $n_c(n_c = 1/a_0^2)$ for different layers of BP. The relation between ratio d^*/d and dimensionless parameter $n^{1/2}d$ (c) without accounting for and (d) taking into account quantum kinetic energy of the charge carriers. The solid curves show the theoretical prediction for three devices. The square, circle, and diamond symbols represent the experimental data. The inset shows the enlarged fitting between the experimental and theoretical values.

negative compressibility of few-layer BP is observed in a region where $n^{-1/2}$ is relatively large and the Coulomb interaction dominates.

Aside from the Coulomb interaction among the carriers, other factors may also contribute to the observed negative compressibility. One possible factor is the frequency-dependent dielectric constant of the BN flakes. Larger geometric capacitance C_g is generated when the dielectric constant of BN thin layers increases with decreased excitation frequency; hence, C_t is enhanced. However, as shown in Figs. 2(b)–2(d), the measured total capacitances at different low excitation frequencies for all three samples converge when the gate voltage is sufficiently large, which yields the same saturated values of C_g at different excitation frequencies. Hence, capacitance enhancement is not caused by the frequency-dependent dielectric constant of BN layers. Another possible capacitance enhancement factor is excitation of localized electronic states in BP at low excitation frequencies. These localized states, which originate from defects or impurities, require a longer time (a smaller excitation frequency) to become excited. At low excitation frequencies, the excited localized states near the band edge could exhibit peaklike features in capacitance spectroscopy [43,44], which may be mistaken for the negative compressibility phenomena. However, the most distinct difference between them is that the peaklike capacitance features induced by localized states never exceed geometric capacitance C_g, disagreeing with experimental observations.

V. CONCLUSIONS

Capacitance enhancement is discovered in high-quality BN-BP-BN heterostructures with few-layer graphene as terminal electrodes at sufficiently low temperatures and relatively low excitation frequencies. Negative electronic compressibility is evident near the band edge of few-layer BP. The negative compressibility observed proves the strong Coulomb interactions in few-layer BP in the low-carrier-density-regime limit. Capacitance enhancement enables switching transistors at small gate voltages. High-quality BN-BP-BN heterostructures with negative compressibility also suggest potential applications of atomically thin materials for low-power nanoelectronics and optoelectronics.

ACKNOWLEDGMENTS

The authors are grateful for fruitful discussions about the capacitance measurement technique with Prof. H. B. Chan from the Physics Department of the Hong Kong University of Science and Technology. Financial support from the Research

Grants Council of Hong Kong (Projects No. 16302215, No. HKU9/CRF/13G, No. 604112, and No. N_HKUST613/12) and the Guangdong Natural Science Funds for Distinguished Young Scholars (Grant No. 2015A030306044) and technical support from the Raith-HKUST Nanotechnology Laboratory for the electron-beam lithography facility at MCPF (Project No. SEG_HKUST08) are hereby acknowledged.

Y.W. and X.C. contributed equally to this work.

[1] S. V. Kravchenko, D. A. Rinberg, S. G. Semenchinsky, and V. M. Pudalov, Phys. Rev. B **42**, 3741 (1990).
[2] R. C. Ashoori and R. H. Silsbee, Solid State Commun. **81**, 821 (1992).
[3] S. C. Dultz and H. W. Jiang, Phys. Rev. Lett. **84**, 4689 (2000).
[4] G. Allison, E. A. Galaktionov, A. K. Savchenko, S. S. Safonov, M. M. Fogler, M. Y. Simmons, and D. A. Ritchie, Phys. Rev. Lett. **96**, 216407 (2006).
[5] A. K. Jonscher and M. N. Robinson, Solid State Electron. **31**, 1277 (1988).
[6] S. Ilani, L. A. K. Donev, M. Kindermann, and P. L. McEuen, Nat. Phys. **2**, 687 (2006).
[7] X. L. Chen, L. Wang, W. Li, Y. Wang, Y. He, Z. Wu, Y. Han, M. Zhang, W. Xiong, and N. Wang, Appl. Phys. Lett. **102**, 203103 (2013).
[8] S. Larentis, J. R. Tolsma, B. Fallahazad, D. C. Dillen, K. Kim, A. H. MacDonald, and E. Tutuc, Nano Lett. **14**, 2039 (2014).
[9] L. Li, C. Richter, S. Paetel, T. Kopp, J. Mannhart, and R. C. Ashoori, Science **332**, 825 (2011).
[10] J. P. Eisenstein, L. N. Pfeiffer, and K. W. West, Phys. Rev. Lett. **69**, 3804 (1992).
[11] A. L. Efros, F. G. Pikus, and V. G. Burnett, Phys. Rev. B **47**, 2233 (1993).
[12] J. P. Eisenstein, L. N. Pfeiffer, and K. W. West, Phys. Rev. B **50**, 1760 (1994).
[13] A. I. Khan, K. Chatterjee, B. Wang, S. Drapcho, L. You, C. Serrao, S. R. Bakaul, R. Ramesh, and S. Salahuddin, Nat. Mater. **14**, 182 (2015).
[14] V. Podzorov, M. E. Gershenson, C. Kloc, R. Zeis, and E. Bucher, Appl. Phys. Lett. **84**, 3301 (2004).
[15] B. Radisavljevic, A. Radenovic, J. Brivio, V. Giacometti, and A. Kis, Nat. Nanotechnol. **6**, 147 (2011).
[16] Q. H. Wang, K. Kalantar-Zadeh, A. Kis, J. N. Coleman, and M. S. Strano, Nat. Nanotechnol. **7**, 699 (2012).
[17] X. Xu, W. Yao, D. Xiao, and T. F. Heinz, Nat. Phys. **10**, 343 (2014).
[18] X. Cui, G. Lee, Y. Kim, G. Arefe, P. Huang, C. Lee, D. Chenet, X. Zhang, L. Wang, F. Ye, F. Pizzocchero, B. Jessen, K. Watanabe, T. Taniguchi, D. Muller, T. Low, P. Kim, and J. Hone, Nat. Nanotechnol. **10**, 534 (2015).
[19] R. Fei and L. Yang, Nano Lett. **14**, 2884 (2014).
[20] S. P. Koenig, R. A. Doganov, H. Schmidt, A. H. Castro Neto, and B. Özyilmaz, Appl. Phys. Lett. **104**, 103106 (2014).
[21] L. Li, Y. Yu, G. J. Ye, Q. Ge, X. Ou, H. Wu, D. Feng, X. H. Chen, and Y. Zhang, Nat. Nanotechnol. **9**, 372 (2014).
[22] H. Liu, A. T. Neal, Z. Zhu, Z. Luo, X. Xu, D. Tománek, and P. D. Ye, ACS Nano **8**, 4033 (2014).
[23] J. Qiao, X. Kong, Z. Hu, F. Yang, and W. Ji, Nat. Commun. **5**, 4475 (2014).
[24] Y. Cao, A. Mishchenko, G. Yu, K. Khestanova, A. Rooney, E. Prestat, A. Kretinin, P. Blake, M. Shalom, and G. Balakrishnan, Nano Lett. **15**, 4914 (2015).
[25] X. Chen, Y. Wu, Z. Wu, Y. Han, S. Xu, L. Wang, W. Ye, T. Han, Y. He, Y. Cai, and N. Wang, Nat. Commun. **6**, 8315 (2015).
[26] L. Li, G. Ye, V. Tran, R. Fei, G. Chen, H. Wang, J. Wang, K. Watanabe, T. Taniguchi, L. Yang, X. Chen, and Y. Zhang, Nat. Nanotechonl. **10**, 608 (2015).
[27] N. Gillgren, D. Wickramaratne, Y. Shi, T. Espiritu, J. Yang, J. Hu, J. Wei, X. Liu, Z. Mao, K. Watanabe, T. Taniguchi, M. Bockrath, Y. Barlas, R. Lake, and C. Lau, 2D Mater. **2**, 011001 (2015).
[28] H. Yuan, X. Liu, F. Afshinmanesh, W. Li, G. Xu, J. Sun, B. Lian, A. Curto, G. Ye, Y. Hikita, Z. Shen, S. Zhang, X. Chen, M. Brongersma, H. Hwang, and Y. Cui, Nat. Nanotechnol. **10**, 707 (2015).
[29] E. Stern, R. Wagner, F. J. Sigworth, R. Breaker, T. M. Fahmy, and M. A. Reed, Nano Lett. **7**, 3405 (2007).
[30] B. Skinner and B. I. Shklovskii, Phys. Rev. B **82**, 155111 (2010).
[31] L. Wang, I. Meric, P. Y. Huang, Q. Gao, Y. Gao, H. Tran, T. Taniguchi, K. Watanabe, L. M. Campos, D. A. Muller, J. Guo, P. Kim, J. Hone, K. L. Shepard, and C. R. Dean, Science **342**, 614 (2013).
[32] S. Sugai and I. Shirotani, Solid State Commun. **53**, 753 (1985).
[33] F. Xia, H. Wang, and Y. Jia, Nat. Commun. **5**, 4458 (2014).
[34] S. Zhang, J. Yang, R. Xu, F. Wang, W. Li, M. Ghufran, Y. Zhang, Z. Yu, G. Zhang, Q. Qin, and Y. Lu, ACS Nano **8**, 9590 (2014).
[35] See Supplemental Material at http://link.aps.org/supplemental/10.1103/PhysRevB.93.035455 for the comparison between this structure using graphene as a terminal with two other capacitor structures without graphene where BN is etched by a chemical method and the BN-BP interface can be contaminated by polymers.
[36] A. Avsar, I. J. Vera-Marun, J. Y. Tan, K. Watanabe, T. Taniguchi, A. H. Castro Neto, and B. Özyilmaz, ACS Nano **9**, 4138 (2015).
[37] S. Luryi, Appl. Phys. Lett. **52**, 501 (1988).
[38] J. Xia, F. Chen, J. Li, and N. Tao, Nat. Nanotechnol. **4**, 505 (2009).
[39] S. Ilani, A. Yacoby, D. Mahalu, and H. Shtrikman, Science **292**, 1354 (2001).
[40] H. Asahina and A. Morita, J. Phys. C **17**, 1839 (1984).
[41] M. S. Bello, E. I. Levin, B. I. Shklovskii, and A. L. Efros, Sov. Phys. JETP **80**, 822 (1981).
[42] B. Skinner and M. M. Fogler, Phys. Rev. B **82**, 201306(R) (2010).
[43] M. M. Ugeda, I. Brihuega, F. Guinea, and J. M. Gómez-Rodríguez, Phys. Rev. Lett. **104**, 096804 (2010).
[44] L. Wang, X. Chen, W. Zhu, Y. Wang, C. Zhu, Z. Wu, Y. Han, M. Zhang, W. Li, Y. He, and N. Wang, Phys. Rev. B **89**, 075410 (2014).